ISSN 1674-1056
http://cpb.iphy.ac.cn
http://iopscience.iop.org/cpb
中国物理 B
Chinese Physics
中国物理 Chinese Physics B

Transport properties of doped Bi_2Se_3 and Bi_2Te_3 topological insulators and heterostructures

Zhen-Hua Wang(王振华), Xuan P A Gao(高翾), Zhi-Dong Zhang(张志东)

Citation: Chin. Phys. B . 2018, 27(10): 107901. **doi:** 10.1088/1674-1056/27/10/107901

Journal homepage: http://cpb.iphy.ac.cn; http://iopscience.iop.org/cpb

What follows is a list of articles you may be interested in

Graphene/Mo_2C heterostructure directly grown by chemical vapor deposition

Rongxuan Deng(邓荣轩), Haoran Zhang(张浩然), Yanhui Zhang(张燕辉), Zhiying Chen(陈志莹), Yanping Sui(隋妍萍), Xiaoming Ge(葛晓明), Yijian Liang(梁逸俭), Shike Hu(胡诗珂), Guanghui Yu(于广辉), Da Jiang(姜达)

Chin. Phys. B . 2017, 26(6): 067901. **doi:** 10.1088/1674-1056/26/6/067901

Interactions between vacancies and prismatic Σ3 grain boundary in α-Al_2O_3: First principles study

Fei Wang(王飞), Wen-Sheng Lai(赖文生), Ru-Song Li(李如松), Bin He(何彬), Su-Fen Li(黎素芬)

Chin. Phys. B . 2016, 25(6): 066804. **doi:** 10.1088/1674-1056/25/6/066804

Domain boundaries in silicene: Density functional theory calculations on electronic properties

Xiao Hong-Jun, Zhang Li-Zhi, Du Shi-Xuan, Gao Hong-Jun

Chin. Phys. B . 2015, 24(8): 086806. **doi:** 10.1088/1674-1056/24/8/086806

Light-extraction efficiency and forward voltage in GaN-based light-emitting diodes with different patterns of V-shaped pits

Wang Min-Shuai, Huang Xiao-Jing

Chin. Phys. B . 2013, 22(8): 086803. **doi:** 10.1088/1674-1056/22/8/086803

The properties of transparent conducting molybdenum-doped ZnO films grown by radio frequency magnetron sputtering

Xiu Xian-Wu, Zhao Wen-Jing

Chin. Phys. B . 2012, 21(6): 066802. **doi:** 10.1088/1674-1056/21/6/066802

TOPICAL REVIEW — Spin manipulation in solids

Transport properties of doped Bi_2Se_3 and Bi_2Te_3 topological insulators and heterostructures*

Zhen-Hua Wang(王振华)[1,†], Xuan P A Gao(高翾)[2], and Zhi-Dong Zhang(张志东)[1]

[1] Shenyang National Laboratory for Materials Science, Institute of Metal Research, Chinese Academy of Sciences, Shenyang 110016, China
[2] Department of Physics, Case Western Reserve University, Cleveland, Ohio 44106, USA

(Received 23 April 2018; revised manuscript received 7 August 2018; published online 10 September 2018)

In this review article, the recent experimental and theoretical research progress in Bi_2Se_3- and Bi_2Te_3-based topological insulators is presented, with a focus on the transport properties and modulation of the transport properties by doping with nonmagnetic and magnetic elements. The electrical transport properties are discussed for a few different types of topological insulator heterostructures, such as heterostructures formed by Bi_2Se_3- and Bi_2Te_3-based binary/ternary/quaternary compounds and superconductors, nonmagnetic and magnetic metals, or semiconductors.

Keywords: transport properties, interfaces, heterostructures, nanostructures, doping, magnetoresistance

PACS: 79.60.Jv, 91.60.Tn, 68.55.Ln, 73.43.Qt **DOI:** 10.1088/1674-1056/27/10/107901

1. Introduction

Topological insulators (TIs) have received increasing attention because of their unique electronic structures, which generally have a gapped bulk band structure and a band inversion induced by spin-orbit interaction that leads to a metallic topological surface state. The recently discovered three-dimensional (3D) TIs show an unconventional electronic phase driven by strong spin–orbit interaction. TI has metallic Dirac fermion surface states that are protected by time-reversal symmetry, resulting in unique properties such as spin momentum locking and prohibited backscattering.[1] 3D TIs have the simplest surface states consisting of a single Dirac cone, which has been proposed theoretically in the stoichiometric compounds Bi_2Se_3, Bi_2Te_3, and Sb_2Te_3.[1] They share the same rhombohedral crystal structure with the space group $D3d5$ ($R3m$), with five atoms in the trigonal unit cell. The presence of Dirac states on the surface of 3D TIs has been confirmed by angle resolved photoemission spectroscopy (ARPES) and scanning tunneling microscopy (STM).[2] These surface states can also be probed by magneto-transport measurements. Numerous studies of magneto-transport measurements also have been performed to prove the existence of surface states by means of analyzing weak anti-localization (WAL) and Shubnikovde Has (SdH) oscillations in Bi_2Te_3 and Bi_2Se_3.[3] The WAL effect can serve as a convenient method for detecting decoupled surface transport in TI thin films. When a bulk Fermi surface coexists with the surface states, the low-field magneto-conductivity is well described by the Hikami–Larkin–Nagaoka equation. When the electron density is decreased, strong evidence is found for independent conducting channels at or near the bottom and top surfaces.[4] However, the contribution of surface state carriers is generally negligible compared with the transport in bulk because the bulk tends to have high intrinsic doping and is thus quite metallic.[5] Therefore, many methods have been explored to control the bulk transport and modulate the transport properties of TIs. For example, a very large tunability in carrier density with a back gate was observed in Bi_2Se_3 thin films. The observed low-field magneto-conductivity resulting from WAL had a gate-voltage dependence when the electron density was reduced to very low values by gating.[6] The bulk properties and WAL effect of Bi_2Se_3 films exhibited thickness dependences over a range of up to five orders of magnitude in thickness.[7] The electronic transport in charge density-tunable microdevices patterned from thin films of TI Bi_2Se_3 has also been studied. These devices exhibited pronounced electric field gating effects, including ambipolar modulation of the resistance.[8] A brief summary of the history of topological insulators and transport experiments on TI films and nanowires can be found in related review papers.[9,10]

In this manuscript, we review the recent experimental and theoretical research efforts in Bi_2Se_3- and Bi_2Te_3-based TIs to achieve control of the Fermi energy (e.g., tuning the Fermi energy into the bulk band gap) by synthesizing ternary/quaternary compounds, gating, or doping with nonmagnetic and magnetic elements. We also discuss some of

*Project supported by the National Natural Science Foundation of China (Grant Nos. 51522104, 51590883, 51331006, and KJZD-EW-M05-3) and the National Science Foundation for its financial support under Award DMR-1151534.

†Corresponding author. E-mail: zhwang@imr.ac.cn

© 2018 Chinese Physical Society and IOP Publishing Ltd

the fascinating properties of these modified TIs and various heterostructures based on TIs.

2. Transport properties of TIs modulated by doping

2.1. Doping TIs with magnetic elements

TIs having magnetic ordering have recently attracted interest because of their promising applications in spintronics and many other novel phenomena, such as the magnetic monopole, novel magnetoelectric quantum states, and quantum anomalous Hall effect (QAH) proposed in ferromagnetic TIs.[11,12] The ferromagnetism introduced by magnetic impurities in a TI film can induce a gap in the Dirac surface, making the TI a QAH insulator if the Fermi level lies in the gap. Magnetic dopants can break the time-reversal protection of the Dirac point, which may open up new applications.

Based on first-principles calculations, the tetradymite semiconductors Bi_2Te_3, Bi_2Se_3, and Sb_2Te_3 are predicted to form magnetically ordered insulator states when doped with transition metal elements (such as Cr or Fe).[11] Much effort has been spent to prepare TIs doped with transition metal elements. Flakes of $Cr_{0.15}(Bi_{0.1}Sb_{0.9})_{1.85}Te_3$ give strong ferromagnetic loops with a T_C of $\sim$ 13 K. Anomalous Hall resistance is observed, indicating obvious suppression because of electron–phonon interactions.[13] Ferromagnetism is observed in TI $Co_{0.08}Bi_{1.92}Se_3$ single crystals. However, the anomalous second ferromagnetic phase transition is indicated by the complicated ferromagnetic ordering below 30 K.[14] The magnetization coming from individual Co atoms deposited on the surface can disrupt the spin coherence of the carriers in the TI Bi_2Te_3 because of the hybridization of Co with the surface states, while in Bi_2Se_2Te, the spin texture remains unperturbed because of the Se–Te disorder of localized magnetic moments in the distorted adsorption geometry.[15] Fe-doped Bi_2Se_3 single nanowires give direct evidence of spontaneous magnetization, with a T_C of $\sim$ 40 K.[16] Locally manipulating the electronic states of Fe dopants in Bi_2Se_3 crystals gives evidence that the specific impurity neighborhood and the position of the Fermi energy have to be taken into account when considering electron scattering from the disorder in TIs.[17] A single-phase crystal structure can be obtained for $(Cr_xSb_{1-x})_2Te_3$ with x up to 0.44, and composition analysis reveals that Cr replaces Sb. A ferromagnetic state with a $T_C \sim 250$ K in $(Cr_{0.44}Sb_{0.56})_2Te_3$ films has been reported, which is the highest T_C observed in magnetically doped TIs so far.[18] A systematic study of V-doped Bi_2Se_3 films reveals the crucial role of topological surface states in ferromagnetic coupling.[19]

The ferromagnetism order is achieved in TI, and the enhanced ferromagnetism with reduced carrier density can support the QAH phase in two-dimensional (2D) thin films of such systems. The QAH effect in Cr-doped topological insulators has been calculated, showing that Sb_2Te_3 is a better QAH-effect TI than Bi_2Se_3 or Bi_2Te_3.[20] It has also been proposed that Mo and Cr co-doping can enlarge the spin splitting of the topological surface states of Sb_2Te_3 and $(Bi,Sb)_2Te_3$, so that the QAHE can persist to higher temperatures. The temperature of the QAH effect also can be significantly increased by co-doping Cr and V magnetic elements in $(Bi,Sb)_2Te_3$ TIs.[21] The electric field has a strong effect on the magnetic order for Cr-doped $Bi_2(Se_xTe_{1-x})_3$ with the application of a gate voltage. Theoretical calculations show that the electronic energy level shift in a perpendicular electric field is due to the Stark effect,[22] so the best way to see the QAH effect in experiments is measuring the Hall conductance by tuning the chemical potential with the gate voltage. The hysteretic magneto-conductance has been investigated, and butterfly-shaped hysteresis characteristics are observed as the applied field increases. This hysteresis is attributed to the formation of gapless chiral domain wall bound states during a magnetic-field sweep. This phenomenon has also been studied theoretically, providing a link between microscopic magnetization dynamics and butterfly hysteresis.[23] The QAH effect is observed experimentally in magnetic thin films of Cr-doped $(Bi,Sb)_2Te_3$.[24,25] At zero magnetic field, the anomalous Hall resistance reaches the predicted quantized value by gate tuning, with an obvious drop in the longitudinal resistance. The longitudinal resistance vanishes under a strong magnetic field, whereas the Hall resistance remains at the quantized value. The experimental results illustrate a method to develop topological quantum electronic and spintronic devices by the realization of the QAH effect, which does not require a magnetic field.

2.2. Doping TIs with nonmagnetic elements

A 3D TI is a novel state of matter characterized by two-dimensional (2D) metallic Dirac states on its surface. However, the bulk has many native defects, such as the Se vacancy (V_{Se}) and the Bi antisite (Bi_{Se}), which means that the bulk carriers from defects dominate over the surface electrons.[26] To verify the topological nature of the surface states, Bi-based chalcogenides such as Bi_2Se_3, Bi_2Te_3, Sb_2Te_3, and their combined/mixed compounds have been intensively studied, and some novel properties, such as the quantum Hall effect and superconductivity, have been reported.

Some effective methods to reduce the effect of bulk carriers on surface states include forming multicomponent compounds and gating.[27–33] The different kinds of defects at the surface of a $(Bi_{0.53}Sb_{0.47})_2Te_3$ TI thin film have been ana-

lyzed, finding the largest localized voltage drop to be located at domain boundaries.[27] The quantum Hall effect on the surface Dirac states in $(Bi_{1-x}Sb_x)_2Te_3$ films can be realized with electrostatic gate-tuning of the Fermi level in the bulk band gap under magnetic fields.[28] Resistivity anisotropy induced by an in-plane magnetic field has been observed in dual-gated bulk-insulating $Bi_{2-x}Sb_xTe_3$ thin films, which show a novel planar Hall effect from the TI surface.[29] The dominant charge carrier changed from n-type to p-type at approximately $x = 0.7$, indicating that the Fermi level can be controlled across the Dirac point. The ambipolar field effect from surface state conduction has been achieved in $Bi_2(Te_{1-x}Se_x)_3$ nanoribbons by applying a back gate voltage.[30,31] Additionally, the helicity-dependent photocurrent in $(Bi_{1-x}Sb_x)_2Te_3$ thin films has been studied synthetically, and the circular photo-galvanic effect has been identified as the dominant mechanism. Strong interlayer interference and coupling of bulk carriers with surface states are observed for all concentrations of Sb at low temperatures.[34,35] The optical properties of thin films of $Bi_2(Te_{1-x}Se_x)_3$ have been investigated using a combination of infrared ellipsometry. The energy of the onset of direct interband transitions exhibits a maximum in Bi_2Te_2Se films, indicating the crossover of the direct interband transitions.[36] The linear magnetoresistance behavior has been shown to be a competition between the bulk insulating states and the metallic surface states.[37] Tuning the Landau levels of the Dirac cones in the top and bottom topological surface states independently can be realized in $BiSbTeSe_2$ by employing both top- and back-gate electric fields at high magnetic field, forming charge puddles as a result of the strong Coulomb disorder.[32,33]

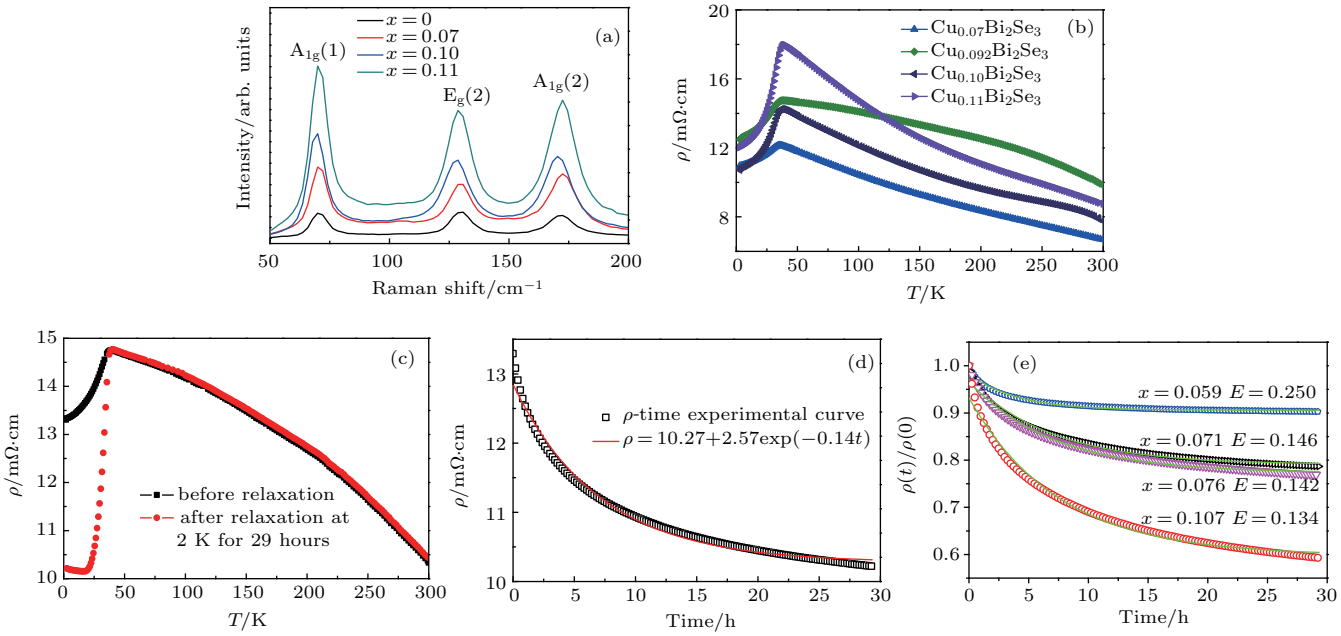


Fig. 1. (color online) (a) Raman spectra of $Cu_xBi_2Se_3$ film samples with $x = 0$, 0.07, 0.10, and 0.11. (b) The resistivity of $Cu_xBi_2Se_3$ films with high Cu concentration dependence on temperature. (c) Temperature dependence of resistivity of $Cu_{0.076}Bi_2Se_3$ (black square) and after (red circle) relaxation at 2 K for 29 h. (d) Time dependence of resistivity of $Cu_{0.076}Bi_2Se_3$ at 2 K over the relaxation process of 29 h. (e) Time dependence of resistivity of $Cu_xBi_2Se_3$ with various Cu concentrations ($x = 0.059$, 0.071, 0.076, 0.107) at 2 K. Solid green lines are best fits. Modified from Li *et al.*, Ref. [47]

The surface state properties of TIs also can be improved by doping other elements, such as Ca, In, and Cu.[38–47] Few-layer crystals of Bi_2Se_3 have sufficiently low bulk carrier density after doping with Ca, which leads to gate voltage-tunable surface conduction.[38] A quantum phase transition from the topological to a trivial insulating phase is achieved in $(Bi_{1-x}In_x)_2Se_3$ film by In doping onto the Bi site.[39] Single-crystalline $(Bi_{1-x}In_x)_2Se_3$ shows quantum oscillations manifesting the nontrivial transport and high mobility.[40] Because of the topological phase transition-enhanced interface coupling near the topological critical point in $(Bi_{0.92}In_{0.08})_2Se_3$, the in-plane negative magneto-resistance emerges and survives up to room temperature.[41] Recently, ARPES results indicated that Cu predominantly intercalates into the van der Waals gap when the Cu concentration is at low level, while with further doping, Cu can replace Bi, causing the saturation of the carrier concentration.[42] Cu can reduce the bulk carrier density of Bi_2Se_3 by compensating for native defects, such that the resistivity is changed from metallic to insulating-like behavior.[43–45] Moreover, Cu can intercalate in the van der Waals gaps between the Bi_2Se_3 layers, which has been investigated by Raman spectroscopy.[46,47] The peaks of $E_g(2)$ and $A_{1g}(2)$ modes will shift to lower frequencies if Cu intercalates between the layers of Bi_2Se_3. However, the $E_g(2)$

and $A_{1g}(2)$ modes are expected to shift to higher frequencies when Bi is substituted by Cu. As shown in Fig. 1(a), $E_g(2)$ and $A_{1g}(2)$ mode peaks first shift to lower frequencies at low Cu concentrations, and then shift to higher frequencies with further increasing Cu concentration. This result indicates that Cu atoms occupy the intercalative sites between the layers at low Cu concentrations and take the substitutional sites of Bi atoms gradually with increasing Cu concentration. As shown in Fig. 1(b), an insulator–metal transition below ~ 37 K is observed in $Cu_xBi_2Se_3$ films with increasing Cu concentration, which is due to electron delocalization resulting from strong hybridization between Cu^+ and Cu^{2+} conduction bands.[47] When Cu intercalates into the van der Waals gap, it can donate as a Cu^+ state, and the substituted Cu is in the Cu^{2+} state. Meanwhile, a relaxation behavior in the time dependence of resistivity is also observed because of the electron delocalization.[47] The temperature dependence of resistivity at zero magnetic field of $Cu_xBi_2Se_3$ ($x = 0.076$) before and after relaxation at 2 K is shown in Fig. 1(c). The kink in resistivity at 37 K is more pronounced after stabilizing at low temperature for a long time, and the two resistivity curves show the same behavior above 37 K. As shown in Fig. 1(d), the resistivity relaxation process with time at 2 K has also been investigated. The red line is the fitting curve. In addition, the dependence of resistivity with time at 2 K for $Cu_xBi_2Se_3$ films with various Cu concentrations is shown in Fig. 1(e). As the Cu concentration increases, the relaxation rate E decreases; that is, relaxation becomes slower.

Cu-intercalated $Cu_xBi_2Se_3$ shows superconductivity, making it a promising candidate for bulk topological superconductors.[46,48,49] Odd-parity nematic superconductivity is found in $Cu_xBi_2Se_3$ from bulk thermodynamic evidence, in which the nematicity emerges in the superconducting gap amplitude.[49] The superconductivity of Cu-doped Bi_2Se_3 is induced by dopant atoms intercalated in van der Waals gaps.[50] However, Sr atoms doped at interstitial locations are most likely to be responsible for the emergence of superconductivity in Sr-doped Bi_2Se_3, instead of those intercalated in van der Waals gaps. Remarkably stable re-emergent superconductivity is observed in $Sr_xBi_2Se_3$ at high pressure, concurrent with a structural phase transition.[51,52] A nodal superconducting gap is observed in $Nb_{0.25}Bi_2Se_3$, consistent with odd-parity Cooper pairing.[53,54] The superconducting transition temperature T_C continuously increases with pressure, which may be attributable to an electronic structure composed of multiple bands.[55] A Nb-doped Bi_2Se_3 superconductor with a trigonal crystal structure has been discovered, providing direct evidence that the superconducting magnetic response couples strongly to the underlying trigonal crystal symmetry.[56]

2.3. Transport properties of TIs modulated by others parameters

TI films are promising materials for optoelectronics because of their strong optical absorption and the thickness-dependent band gap of the topological surface states. Novel polarization-dependent photocurrent in photodetectors based on TI Bi_2Te_3 films under irradiation of linearly polarized light has been observed in experiments.[57] A significantly improved optoelectronic performance resulting from strain has been demonstrated using first-principles Hamiltonian calculation. The optical absorption of Bi_2Se_3 films with variable thickness is theoretically predicted to be effectively tuned by the application of uniaxial strain.[58] The intriguing electrical transport properties of compressed Sb_2Te_3 has been reported. A significant anomaly in the Hall coefficient at 3.4 GPa reveals an electronic topological transition. In addition, a semiconductor to semi-metal transition is observed at approximately 9.0 GPa because of the pressure-driven overlapping band.[59]

The linear magneto-resistance (MR) effect is an interesting topic because of its potential applications. The linear MR of single-crystalline TIs in a perpendicular field is attributed to the 2D gapless topological surface states and is of quantum origin; alternatively, it may be due to the charge inhomogeneity and conductivity fluctuation.[60,61] Granular films of Bi_2Te_3 nanoplates provide definite evidence for a sample's physical or structural inhomogeneity as the origin of linear MR.[62] In Bi_2Te_3 films formed with Bi_2Te_3 nanoplates, a typical morphology is shown in Figs. 2(a)–2(c). As a semi-quantitative way to characterize the granularity of the film, six samples were selected. Figure 2(d) shows the number of nanoplates counted over an area of 20 μm×20 μm versus the average mobility. The results indicate that the higher density of nanoplates in the film leads to higher mobility because of the improved connectivity of the network. Three typical Bi_2Te_3 nanoplate film samples with linear MR effects are shown in Figs. 2(e)–2(g). The magnitude of the MR decreases with increasing temperature. Putting all the $[R(B) - R(0)]/R(0)$, granularity, and temperature data for the six samples together in the same graph, a close correlation between the linear MR, average mobility, and the sample's uniformity is revealed over a broad range of parameter space, as shown in Fig. 2(h). These results show that the linear MR can be attributed to large spatial fluctuations in the conductivity of the material, which is clear evidence for the phenomenological model of Parish–Littlewood. The observed linear MR in Bi_2Se_3 thin films is dominated by the inverse disorder parameter, which may be due to the very small carrier mobility. It is possible to tune Dirac surface states by applying external strain to single-crystalline Bi_2Se_3 nanowires. Surface states can be enhanced or destroyed by strain in the vicinity of grain boundaries on the surface of epitaxial Bi_2Se_3 thin films.[63–65]

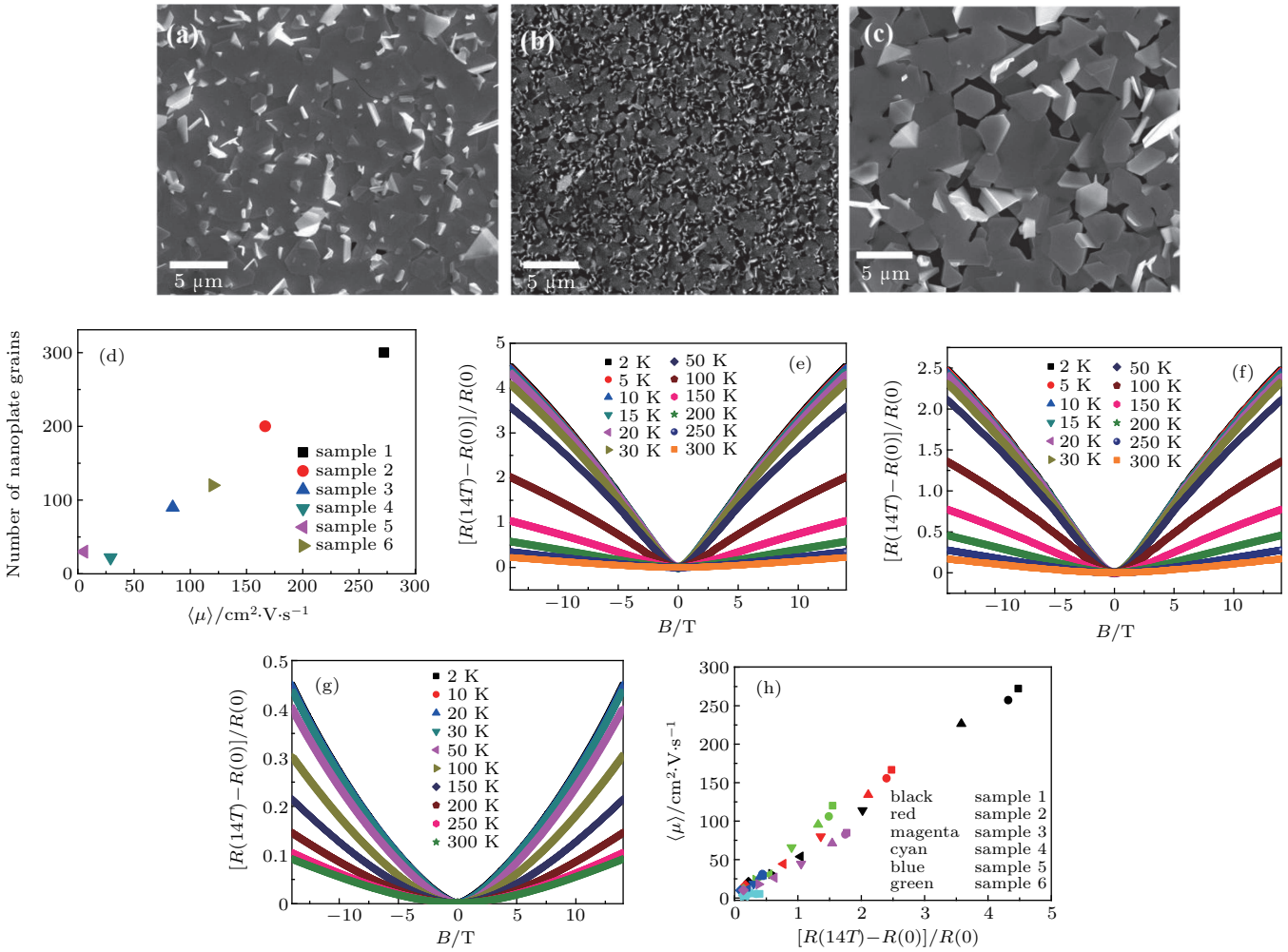


Fig. 2. (color online) (a)–(c) SEM image of Bi_2Te_3 film samples formed with various Bi_2Te_3 nanoplates. (d) Number of nanoplate grains per 20 μm ×20 μm area versus the average mobility of the film. (e)–(g) Magneto-resistance $[R(B)-R(0)]/R(0)$ as a function of magnetic field at various temperatures for three different samples. (h) The relationship between mobility and $[R(14T)-R(0)]/R(B=0)$ for various samples with different granularities. Modified from Wang *et al.*, Ref. [64].

3. Transport properties of TIs modulated by heterostructuring

3.1. TI/magnetic insulator (MI) heterostructures

The interface between a TI and an MI exhibits an interesting interplay of topological Dirac electrons and magnetism. The MI can be ferromagnetic or antiferromagnetic. The magnetic proximity effect between the TI and MI is considered to have great potential in spintronics. A promising example is the realization of the quantum anomalous Hall effect. Domain-wall Majorana bound states are predicted at the TI/MI interface.

As has been shown recently, based on ab initio calculations, Cr-doped $(Bi,Sb)_2Te_3/GdI_2$ heterostructures are predicted to be QAH insulators with a nontrivial band gap. The breaking of time-reversal invariance by the magnetic order generates a nonzero Chern number that in turn leads to a Berry phase and a magnetoelectric effect. Moreover, it is predicted that a 3D QAH insulator could be realized in a $(Bi_{2/3}Cr_{1/3})_2Te_3/GdI_2$ superlattice. The magnetoelectric effect of the fluctuating electric field becomes nonlocal when the system is in the presence of a long-range Coulomb interaction between the Dirac electrons.[66,67] The transport properties of heterostructures formed by various types of MI/TI have been investigated.[68,69] High-quality antiferromagnetic MnSe films have been grown on a Bi_2Se_3 surface layer-by-layer, which reveals that an energy gap appears at the Dirac point of the original Bi_2Se_3 surface, possibly by breaking the time-reversal symmetry on the Bi_2Se_3 surface because of the magnetic proximity effect from MnSe.[68] A strong suppression of the weak antilocalization effect is observed in antiferromagnetic NiO/Bi_2Se_3 and attributed to the strong magnetic exchange field from the Ni electrons.[69] Giant spin-orbit torque-driven magnetization switching in NiFe/Bi_2Se_3 heterostructures has been directly shown at room temperature using a magneto-optic Kerr effect microscope.[70] Magnetic manipulation of the surface states on a single facet of a rectangular TI nanowire has been realized in Bi_2Te_3 nanowire/Fe_3O_4 substrates, breaking the local time-reversal symmetry and en-

hancing the gapping of the one-dimensional spectrum with a coupled ferromagnetic insulator substrate.[71] The transport properties of heterostructures formed by multilayers have also been studied theoretically, such as magnetic 3D TI thin films sandwiched between slabs of normal insulator, and two ferromagnetic insulators separated by a TI thin film, indicating that the spin-polarization magnitude is strongly dependent on the magnetic insertion position in the film and the particular electronic states of the TI contributing to the proximity effect can be directly identified through the coupling between two ferromagnetic insulators.[72,73] Proximity effect-induced superconductivity has been observed in epitaxial TI Bi_2Se_3 thin films grown on superconducting $NbSe_2$ single crystals.[74] The superconducting transition temperature can be increased by pressure-induced enhanced coupling of the $Fe_{1+y}Te$ interfacial layer with the Bi_2Te_3 surface state.[75] Additionally, the chiral Majorana fermion mode is suggested in the hybrid system of a QAH TI thin film coupled with a superconductor.[76]

Emergent interfacial magnetic phenomena can be realized through artificial structural engineering by constructing heterostructures in MI/FM-IT, such as antiferromagnetic CrSb/ferromagnetic Cr-doped $(Bi,Sb)_2Te_3$,[77] in which proximity effects are shown to induce an interfacial spin texture modulation and establish an effective long-range exchange coupling. Dramatic enhancement of proximity exchange coupling has been reported in an MI/magnetic-TI $EuS/Sb_{2-x}V_xTe_3$ hybrid heterostructure,[78] while the Dirac electron-mediated magnetic proximity effect is observed in TI $(Bi_{0.2}Sb_{0.8})_2Te_3$/MI EuS heterostructures, which can be maximized by applying an electrical back gate.[79] Ferromagnetic resonance-driven spin pumping signals are observed at room temperature in 3D TI thin films-$Y_3Fe_5O_{12}$ heterostructures, where the thin TI films can be Bi_2Se_3 or $(Bi, Sb)_2Te_3$. The results show that the spin-charge conversion efficiency increases dramatically as the TI film thickness increases.[80] The spin current induced by the coupling between the spin-momentum-locked surface states and magnons has been derived theoretically and observed in $(Bi_{0.22}Sb_{0.78})_2Te_3$/permalloy (Py).[81,82] Unidirectional spin Hall resistance is observed in TI/FM heterostructures, including $(Bi,Sb)_2Te_3$/CoFeB and Bi_2Se_3/CoFeB bilayers. The original Dirac cone is destroyed and an interface state formed near the Fermi level as a result of the strong hybridization with the FM states.[83,84] The proximity effect is described by the exchange interaction between the delocalized electrons of the surface and bulk states in the Bi_2Se_3 film and localized Fe electrons in the $Y_3Fe_5O_{12}$ film.[85] The temperature coefficients of the resistance of a $(Bi_xSb_{1-x})_2Te_3/SrRuO_3$ bilayer are suppressed, indicating the presence of a magnetic proximity effect in the bilayer.[86] Electron transport at the interface between TI and MI with magnetic skyrmions on the top has been investigated theoretically, finding that the skyrmions yield an additional contribution to the anomalous Hall conductivity.[87] Skyrmionium has also been observed in thin ferromagnetic films of $Ni_{80}Fe_{20}$/Cr-doped Sb_2Te_3. The occurrence of skyrmionium is tied to the ferromagnetic state of the topological insulator.[88] It has been shown that charge current flowing in-plane in a thin film of the topological insulator Bi_2Se_3 at room temperature can generate a strong spin-transfer torque on an adjacent ferromagnetic permalloy ($Ni_{81}Fe_{19}$) thin film, and this effect can be attributed to the topological surface states.[89]

3.2. TI/nonmagnetic materials heterostructures

Recent theories have predicted that the hybridization between graphene and TIs can create nontrivial spin textures in graphene, even leading to quantum spin Hall states.[90,91] A chiral magnetic structure is formed by graphene nanoribbons deposited on Sb_2Te_3 because of the interplay between strong spin-orbit coupling and broken inversion symmetry.[92] The anisotropic spin transport in graphene–Bi_2Se_3 has been revealed by theoretical predictions to be caused by the spin proximity effect, with a dependence of the anisotropy on the geometry of the interface.[93] Figure 3 shows the spin lifetime anisotropy in graphene–Bi_2Se_3 heterostructures with panels (a) and (b) for small and large unit cells, respectively. In the small unit cell, the anisotropy remains negligible far from the graphene Dirac point and reaches values in the hundreds near the Dirac point. Figure 3(b) shows the anisotropy in the large unit cell. Both the tight-binding (TB) fit and the analytical prediction show good agreement with the density functional theory (DFT) results. In this case, the anisotropy is characterized by a strong electron-hole asymmetry.[94] A giant negative anomalous magneto-transport property for graphene–Bi_2Se_3 heterojunctions has been reported, which is enhanced by applying a perpendicular negative magnetic field because of the electronic coupling between graphene and the topological surface state.[94] The spin-polarized current from a TI can be injected into graphene in a van der Waals epitaxial Bi_2Te_2Se–graphene heterostructure, which indicates that spin manipulation can be achieved by purely electrical means.[95]

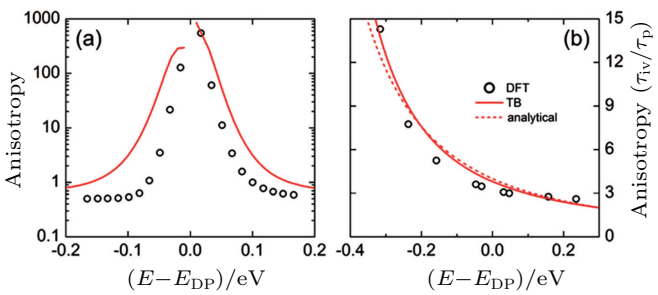


Fig. 3. (color online) Spin lifetime anisotropy of graphene/Bi_2Se_3 heterostructures as a function of energy relative to the graphene Dirac point. Panels (a) and (b) show the anisotropy in small and large unit cells, respectively. Modified from Song *et al.*, Ref. [95].

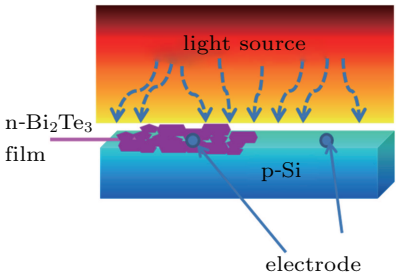


Fig. 4. (color online) Schematic for measuring the photo-properties structure of n-Bi_2Te_3/p-Si junctions. Modified from Wang *et al.*, Ref. [102].

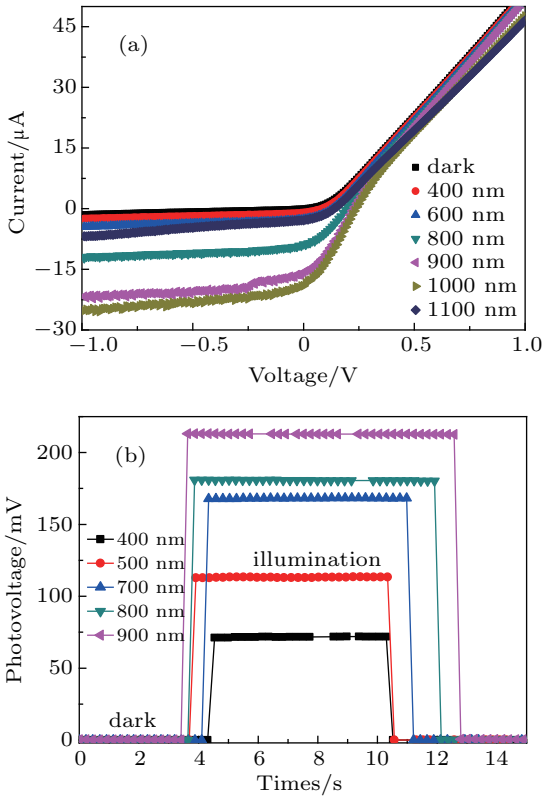


Fig. 5. (color online) (a) The *I*–*V* characteristics of n-Bi_2Te_3/p-Si junctions in the dark and under illumination with various wavelengths of light. (b) The dependence of junction photovoltage on time under light illumination with various wavelengths of light. Modified from Wang *et al.*, Ref. [102].

Vertically stacked p–n junctions can be formed by combining n-type Bi_2Te_3 and p-type Sb_2Te_3 TIs. The surface and bulk transport modes of vertical Bi_2Te_3/Sb_2Te_3 heterostructures are disentangled by measuring magneto-transport with varying relative thicknesses.[96] The thermoelectric conversion capability of lateral heterostructures has been experimentally investigated, consisting of n-type Bi_2Te_2Se and p-type Sb_2Te_3, which showed a high thermoelectric performance at room temperature.[97] P-type Sb_2Te_3/n-type strontium titanate heterostructures exhibit pronounced photovoltaic behavior over a wide range of temperatures because of a strong built-in field at the heterointerface.[98] N-Bi_2Se_3 nanoflake/p-Si nanowire heterojunction devices have been fabricated, showing high performance in the near-infrared region.[99] N-type TI Bi_2Te_3/p-Si junctions demonstrate nonlinear diode-type *I*–*V* characteristics. The schematic for measuring the n-Bi_2Te_3/p-Si junctions' photo-properties is shown in Fig. 4. The photovoltaic effect at various wavelengths for a typical sample is shown in Fig. 5(a). Clear p–n diode properties are found in smooth Bi_2Te_3 films formed with large Bi_2Te_3 nanoplates, which show a good photovoltaic effect with broadband photo-response across the UV, visible, and NIR wavelength range.[100] The photovoltage can be effectively switched on and off while the light source is turned on and off under light illumination with various wavelengths of light, as shown in Fig. 5(b). The Kohn anomalies are observed at the surface of Bi_2Te_3/GaAs, demonstrating important electron–phonon coupling effects.[101] Anomalous photogalvanic effects in $(Bi_{0.5}Sb_{0.5})_2Te_3$/GaAs have been reported, and the helicity-dependent photocurrent can be modulated by the gate voltage.[102]

4. Summary and outlook

In this review paper, we have discussed some of the most exciting and promising research on the characterization and transport properties of TIs modified by doping or heterostructuring. Doping TIs with magnetic elements introduces large magnetic moments and results in high crystal quality with high doping concentrations. The paramagnetic state, ferromagnetic state, and antiferromagnetic state have been observed in TIs doped with rare earth ions, transition metals, and so on. The QAH is proposed in ferromagnetic TIs. The ferromagnetic state with the highest $T_C \sim 250$ K was reported in Cr-doped Sb_2Te_3 films. An insulator-metal transition below ~ 37 K was observed in $Cu_xBi_2Se_3$ films because of electron delocalization resulting from the strong hybridization between Cu^+ and Cu^{2+} conduction bands. The superconductivity of Cu- and Sr-doped Bi_2Se_3 was induced by dopant atoms intercalated in van der Waals gaps or interstitial locations. Heterostructures of TIs with other materials have been studied because their interface exhibits interesting interplay effects. The magnetic proximity effect between a TI and MI can induce many interesting properties, such as the chiral Majorana fermion mode, which was suggested in an AQH TI thin film coupled with a superconductor; the spin current induced by coupling between the spin-momentum-locked surface state and magnons; and skyrmions, which make an additional contribution to the anomalous Hall conductivity at the interface between TI and MI with magnetic skyrmions. Topological crystalline insulators (TCIs), as a new member of the TI family, have received attention recently because their surface carries an even number of Dirac cones protected by crystalline symmetry, which is different from the well-known TIs. An even number of Dirac surface states for TCIs leads to many fascinating topological phenomena in theory.[103,104] The intermediate valent Kondo insulator SmB_6 is proposed to be a TI, and the low-temperature

conductivity of SmB_6 can be explained by a topologically protected metallic surface state, as expected in TI.[105,106] Many fascinating topological phenomena are waiting to be discovered and investigated with experiments. Many of these novel effects have been investigated theoretically, while experimental studies are more challenging. Therefore, it is necessary to achieve more progress in this area experimentally.

References

[1] Zhang H J, Liu C X, Qi X L, Dai X, Fang Z and Zhang S C 2009 *Nat. Phys.* **5** 438

[2] Chen Y L, Analytis J G, Chu J H, Liu Z K, Mo S K, Qi X L, Zhang H J, Lu D H, Dai X, Fang Z, Zhang S C, Fisher I R, Hussain Z and Shen Z X 2009 *Science* **325** 178

[3] Cha J J, Kong D S, Hong S S, Analytis J G, Lai K and Cui Y 2012 *Nano Lett.* **12** 1107

[4] Chen J, He X Y, Wu K H, Ji Z Q, Lu L, Shi J R, Smet J H and Li Y Q 2011 *Phys. Rev. B* **83** 241304(R)

[5] Cao H L, Venkatasubramanian R, Liu C, Pierce J, Yang H, Hasan M Z, Wu Y and Chen Y P 2012 *Appl. Phys. Lett.* **101** 162104

[6] Chen J, Qin H J, Yang F, Liu J, Guan T, Qu F M, Zhang G H, Shi J R, Xie X C, Yang C L, Wu K H, Li Y Q and Lu L 2010 *Phys. Rev. Lett.* **105** 176602

[7] Kim Y S, Brahlek M, Bansa N, Edrey E, Kapilevich G A, Iida K, Tanimura M, Horibe Y, Cheong S W and Oh S 2011 *Phys. Rev. B* **84** 073109

[8] Steinberg H, Laloë J B , Fatemi V, Moodera J S and Jarillo-Herrero P 2011 *Phys. Rev. B* **84** 233101

[9] Wang Z H, Gao X P A and Zhang Z D 2017 *Outlook Challenges Nano Devices Sensors MEMS* (Springer: Ting Li & Ziv Liu) p. 429

[10] Liu Y, Ma Z, Zhao Y F, Meenakshi S and Wang J 2013 *Chin. Phys. B* **22** 067302

[11] Yu R, Zhang W, Zhang H J, Zhang S C, Dai X and Fang Z 2010 *Science* **329** 61

[12] Lee C H, He R, Wang Z H, Qiu R L J Kumar A, Delaney C, Beck B, Kidd T E, Chancey C C, Sankaran R M, Gao X P A 2013 *Nanoscale* **5** 4337

[13] Zhang S, Li Z G, Pan X C, Wang X F, Song F Q 2015 *Solid State Commun.* **223** 45

[14] Zhang M, Liu L G, Yang H 2016 *J. Alloys Compd.* **678** 463

[15] Martínez-Velarte M C, Kretz B, Moro-Lagares M, Aguirre M H, Riedemann T M, Lograsso T A, Morellón L, Ibarra M R, Garcia-Lekue Arán and Serrate D 2017 *Nano Lett.* **17** 4047

[16] Niu W, Du K, Wang S B, Zhang M H, Gao M, Chen Y D, Liu H, Zhou W, Song F Q, Wang P, Xu Y B, Wang X F, Shen J and Zhang R 2017 *Nano Scale* **9** 12372

[17] Stolyarov V S, Remizov S V, Shapiro D S, Pons S, Vlaic S Aubin H, Baranov D S, Brun C, Yashina L V, Bozhko S I, Cren T, Pogosov W V and Roditchev D 2017 *Appl. Phys. Lett.* **111** 251601

[18] Gupta S, Kanai S, Matsukura F and Ohno H 2017 *Appl. Phys. Exp.* **10** 103001

[19] Zhang L G, Zhao D P, Zang Y Y, Yuan Y H, Jiang G Y, Liao M H, Zhang D, He K, Ma X C and Xue Q K 2017 *APL Mater.* **5** 076106

[20] Kim J, Jhi S H, MacDonald A H and Wu R 2017 *Phys. Rev. B* **96** 140410(R)

[21] Ou Y B, Liu C, Jiang G Y, Feng Y, Zhao D Y, Wu W X, Wang X X, Li W, Song C L, Wang L L, Wang W B, Wu W D, Wang Y Y, He K, Ma X C and Xue Q K 2018 *Adv. Mater.* **30** 1703062

[22] Zhang J, Chang C Z, Tang P Z, Zhang Z C, Feng X, Li K, Wang L L, Chen X, Liu C X, Duan W H, He K, Xue Q K, Ma X C, Wang Y Y 2013 *Science* **339** 1582

[23] Tiwari K L, Coish W A and Pereg-Barnea T 2017 *Phys. Rev. B* **96** 235120

[24] Feng X, Feng Y, Wang J, Ou Y B, Hao Z Q, Liu C, Zhang Z C, Zhang L G, Lin C J, Liao J, Li Y Q, Wang L L, Ji S H, Chen X, Ma X C, Zhang S C, Wang Y Y, He K and Xue Q K 2016 *Adv. Mater.* **28** 6386

[25] Chang C Z, Zhang J, Feng X, Shen J, Zhang Z C, Guo M H, Li K, Ou Y B, Wei P, Wang L L, Ji Z Q, Feng Y, Ji S, Chen X, Jia J F, Dai X, Fang Z, Zhang S C, He K, Wang Y Y, Lu L, Ma X C and Xue Q K 2013 *Science* **340** 167

[26] West D, Sun Y Y, Wang H, Bang J and Zhang S B 2012 *Phys. Rev. B* **86** 121201(R)

[27] Lüpke F, Eschbach M, Heider T, Lanius M, Schüffelgen P, Rosenbach D, von den Driesch N, Cherepanov V, Mussler G, Plucinski L, Grützmacher D, Schneider C M and Voigtländer B 2017 *Nat. Commun.* **8** 15704

[28] Yoshimi R, Tsukazaki A, Kozuka Y, Falson J, Takahashi K S, Checkelský J G, Nagaosa N, Kawasaki M and Tokura Y 2015 *Nat. Commun.* **6** 6627

[29] Taskin A A, Legg H F, Yang F, Sasaki S, Kanai Y, Matsumoto K, Rosch A and Ando Y 2017 *Nat. Commun.* **8** 1340

[30] Satake Y, Shiogai J, Takane D, Yamada K, Fujiwara K, Souma S, Sato T, Takahashi T and Tsukazaki A 2018 *J. Phys.: Condens. Matter* **30** 085501

[31] Wang Z H, Qiu R L J, Lee C H, Zhang Z D and Gao X P A 2013 *ACS Nano* **7** 2126

[32] Li C, de Ronde B, Nikitin A, Huang Y, Golden M S, de Visser A and Brinkman A 2017 *Phys. Rev. B* **96** 195427

[33] Knispel T, Jolie W, Borgwardt N, Lux J, Wang Z, Ando Y, Rosch A, Michely T and Grüninger M 2017 *Phys. Rev. B* **96** 195135

[34] Pan Y, Wang Q Z, Yeats A L, Pillsbury T, Flanagan T C, Richardella A, Zhang H, Awschalom D D, Liu C X and Samarth N 2017 *Nat. Commun.* **8** 1037

[35] Urkude R R, Rawat R and Palikundwar U A 2017 *J. Phys.: Condens. Matter* **29** 495602

[36] Dubroka A, Caha O, Hronček M, Friš P, Orlita M, Holý V, Steiner H, Bauer G, Springholz G and Humlíček J 2017 *Phys. Rev. B* **96** 235202

[37] Singh S, Gopal R K, Sarkar J, Pandey A, Patel B G and Mitra C 2017 *J. Phys.: Condens. Matter* **29** 505601

[38] Checkelsky J G, Hor Y S, Cava R J and Ong N P 2011 *Phys. Rev. Lett.* **106** 196801

[39] Autore M, Giorgianni F, D' Apuzzo F, Gaspare A D, Vecchio I L, Brahlek M, Koirala N, Oh S, Schade U, Ortolanic M and Lupi S 2016 *Nanoscale* **8** 4667

[40] Zhang M, Li Y, Song F, Wang X and Zhang R 2017 *Chin. Phys. B* **26** 127305

[41] Zhang M, Wang H, Mu K, Wang P, Niu W, Zhang S, Xiao G, Chen Y, Tong T, Fu D, Wang X, Zhang H, Song F, Miao F, Sun Z, Xia Z, Wang X, Xu Y, Wang B, Xing D and Zhang R 2018 *ACS Nano* **12** 1537

[42] Tanaka Y, Nakayama K, Souma S, Sato T, Xu N, Zhang P, Richard P, Ding H, Suzuki Y, Das P, Kadowaki K and Takahashi1 T 2012 *Phys. Rev. B* **85** 125111

[43] Chen T S, Chen Q, Schouteden K, Huang W K, Wang X F, Li Z, Miao F, Wang X R, Li Z G, Zhao B, Li S C, Song F Q, Wang J L, Wang B G, Haesendonck C V and Wang G H 2014 *Nat. Commun.* **5** 5022

[44] Brahlek M, Koirala N, Salehi M, Bansal N and Oh S 2014 *Phys. Rev. Lett.* **113** 26801

[45] Li M Z, Wang Z H, Yang L, Gao X P A, Zhang Z D 2017 *J. Phys. Chem. Solids* **x** 1

[46] Hor Y S, Williams A J, Checkelsky J G, Roushan P, Seo J, Xu Q, Zandbergen H W, Yazdani A, Ong N P and Cava R J 2010 *Phys. Rev. Lett.* **104** 057001

[47] Li M Z, Wang Z H, Yang L, Li D, Yao Q R, Rao G H, Gao Xuan P A and Zhang Z D 2017 *Phys. Rev. B* **96** 075152

[48] Kriener M, Segawa K, Ren Z, Sasaki S and Ando Y 2011 *Phys. Rev. Lett.* **106** 127004

[49] Yonezawa S, Tajiri K, Nakata S, Nagai Y, Wang Z, Segawa K, Ando Y and Maeno Y 2017 *Nat. Phys.* **13** 123

[50] Shirasawa T, Sugiki M, Hirahara T, Aitani M, Shirai T, Hasegawa S and Takahashi T 2014 *Phys. Rev. B* **89** 195311

[51] Li Z, Wang M, Zhang D, Feng N, Jiang W, Han C, Chen W, Ye M, Gao C, Jia J, Li J, Qiao S, Qian D, Xu B, Tian H and Gao B 2018 *Phys. Rev. Mater.* **2** 014201

[52] Zhou Y, Chen X, Zhang R, Shao J, Wang X, An C, Zhou Y, Park C, Tong W, Pi L, Yang Z, Zhang C and Zhang Y 2016 *Phys. Rev. B* **93** 144514

[53] Smylie M P, Claus H, Welp U, Kwok W K, Qiu Y, Hor Y S and Snezhko A 2016 *Phys. Rev. B* **94** 180510

[54] Smylie M P, Willa K, Claus H, Snezhko A, Martin I, Kwok W K, Qiu Y, Hor Y S, Bokari E, Niraula P, Kayani A, Mishra V and Welp U 2017 *Phys. Rev. B* **96** 115145

[55] Smylie M P, Willa K, Ryan K, Claus H, Kwok W K, Qiu Y, Hor Y S and Welp U 2017 *Physica C* **543** 58

[56] Asaba T, Lawson B J, Tinsman C, Chen L, Corbae P, Li G, Qiu Y, Hor Y S, Fu L and Li L 2017 *Phys. Rev. X* **7** 011009

[57] Yao J D, Shao J M, Li S W, Bao D H and Yang G W 2015 *Sci. Rep.* **5** 14184

[58] Brems M R, Paaske J, Lunde A M and Willatzen M 2018 *Phys. Rev. B* **97** 081402(R)

[59] Zhang J, Hu T, Yan J, Ke F, Wang J, Cui X, Li X, Ma Y, Yang J and Gao C 2017 *Mater. Lett.* **209** 78

[60] Tang H, Liang D, Qiu Richard L J and Gao X P A 2011 *ACS Nano* **5** 7510

[61] He H T, Liu H C, Li B K, Guo X, Xu Z J, Xie M H and Wang J N 2013 *Appl. Phys. Lett.* **103** 031606

[62] Wang Z H, Yang L, Li X J, Zhao X T, Wang H L, Zhang Z D and Gao X P A 2014 *Nano Lett.* **14** 6510

[63] Wang W J, Gao K H, Li Q L and Li Z Q 2017 *Appl. Phys. Lett.* **111** 232105

[64] Schindler C, Wieg, C, Sichau J, Tiemann L, Nielsch K, Zierold R and Blick R H 2017 *Appl. Phys. Lett.* **111** 171601

[65] Liu Y, Li Y Y, Rajput S, Gilks D, Lari L, Galindo P L, Weinert M, Lazarov V K and Li L 2014 *Nat. Phys.* **10** 294

[66] Xu G, Wang J, Felser C, Qi X L and Zhang S C 2015 *Nano Lett.* **15** 2019

[67] Rex S, Nogueira F S and Sudbø A 2016 *Phys. Rev. B* **93** 014404

[68] Matetskiy A V, Kibirev I A, Hirahara T, Hasegawa S, Zotov A V and Saranin A A 2015 *Appl. Phys. Lett.* **107** 091604

[69] Bhowmick T, Jerng S K, Jeon J H, Roy S B, Kim Y H, Seo J, Kim J S and Chun S H 2017 *Nanoscale* **9** 844

[70] Wang Y, Zhu D, Wu Y, Yang Y, Yu J, Ramaswamy R, Mishra R, Shi S, Elyasi M, Teo K L, Wu Y and Yang H 2017 *Nat. Commun.* **8** 1364

[71] Gooth J, Zierold R, Sergelius P, Hamdou B, Garcia J, Damm C, Rellinghaus B, Pettersson H J, Pertsova A, Canali C, Borg M and Nielsch K 2016 *ACS Nano* **10** 7180

[72] Meńshov V N, Tugushev V V and Chulkov E V 2016 *JETP Lett.* **104** 453

[73] Li M, Cui W, Yu J, Dai Z, Wang Z, Katmis F, Guo W and Moodera J 2015 *Phys. Rev. B* **91** 014427

[74] Dai W, Richardella A, Du R, Zhao W, Liu X, Liu C X, Huang S H, Sankar R, Chou F, Samarth N and Li Q 2017 *Sci. Rep.* **7** 7631

[75] Shen J, Heuckeroth C, Deng Y, He Q, Liu H C, Liang J, Wang J, Sou I K, Schilling J S and Lortz R 2017 *Physica C* **543** 18

[76] He Q L, Pan L, Stern A L, Burks E C, Che X, Yin G, Wang J, Lian B, Zhou Q, Choi E S, Murata K, Kou X, Chen Z, Nie T, Shao Q, Fan Y, Zhang S C, Liu K, Xia J and Wang K L 2017 *Science* **357** 294

[77] He Q L, Kou X, Grutter A J, Yin G, Pan L, Che X, Liu Y, Nie T, Zhang B, Disseler S M, Kirby B J, Ratcliff W, Shao Q, Murata K, Zhu X, Yu G, Fan Y, Montazeri M, Han X, Borchers J A and Wang K L 2017 *Nat. Mater.* **16** 94

[78] Li M, Chang C Z, Kirby B J, Jamer M E, Cui W, Wu L, Wei P, Zhu Y, Heiman D, Li J and Moodera J S 2015 *Phys. Rev. Lett.* **115** 087201

[79] Li M, Song Q, Zhao W, Garlow J A, Liu T H, Wu L, Zhu Y, Moodera J S, Chan M H W, Chen G and Chang C Z 2017 *Phys. Rev. B* **96** 201301(R)

[80] Wang H, Kally J, Lee J S, Liu T, Chang H and Hickey D R 2016 *Phys. Rev. Lett.* **117** 076601

[81] Okuma N and Nomura K 2017 *Phys. Rev. B* **95** 115403

[82] Mendes J B S, Santos O A, Holanda J, Loreto R P, de Araujo C I L, Chang C Z, Moodera J S, Azevedo A and Rezende S M 2017 *Phys. Rev. B* **96** 180415(R)

[83] Lv Y, Kally J, Zhang D, Lee J S, Jamali M, Samarth N and Wang J P 2018 *Nat. Commun.* **9** 111

[84] Hsu Y T, Park K and Kim E A 2017 *Phys. Rev. B* **96** 235433

[85] Kubota Y, Murata K, Miyawaki J, Ozawa K, Onbasli M C, Shirasawa T, Feng B, Yamamoto S, Liu R Y, Yamamoto S, Mahatha S K, Sheverdyaeva P, Moras P, Ross C A, Suga S, Harada Y, Wang K L and Matsuda I 2017 *J. Phys.: Condens. Matter* **29** 055002

[86] Koren G 2018 *Phys. Rev. B* **97** 054405

[87] Araki Y and Nomura K 2017 *Phys. Rev. B* **96** 165303

[88] Zhang S, Kronast F, van der Laan G and Hesjedal T 2018 *Nano Lett.* **18** 1057

[89] Mellnik A R, Lee J S, Richardella A, Grab J L, Mintun P J, Fischer M H, Vaezi A, Manchon A, Kim E A, Samarth N and Ralph D C 2014 *Nature* **511** 449

[90] Kou L, Hu F, Yan B, Wehling T, Felser C, Frauenheim T and Chen C 2015 *Carbon* **87** 418

[91] Jin K H and Jhi S H 2013 *Phys. Rev. B* **87** 075442

[92] Zhang W, Hajiheidari F and Mazzarello R 2017 *Phys. Rev. B* **96** 245413

[93] Song K, Soriano D, Cummings A W, Robles R, Ordejón P and Roche S 2018 *Nano Lett.* **18** 2033

[94] Zhang L, Lin B C, Wu Y F, Wu H C, Huang T W, Chang C R, Ke X, Kurttepeli M, Tendeloo G V, Xu J, Yu D and Liao Z M 2017 *ACS Nano* **11** 6277

[95] Vaklinova K, Hoyer A, Burghard M and Kern K 2016 *Nano Lett.* **16** 2595

[96] Backes D, Huang D, Mansell R, Lanius M, Kampmeier J, Ritchie D, Mussler G, Gumbs G, Grützmacher D and Narayan V 2017 *Phys. Rev. B* **96** 125125

[97] Mashhadi S, Duong D L, Burghard M and Kern K 2017 *Nano Lett.* **17** 214

[98] Sun H, Jiang T, Zang Y, Zheng X, Gong Y, Yan Y, Xu Z, Liu Y, Fang L, Cheng X and He K 2017 *Nanoscale* **9** 9325

[99] Das B, Das N S, Sarkar S, Chatterjee B K and Chattopadhyay K K 2017 *ACS Appl. Mater. Interfaces* **9** 22788

[100] Wang Z H, Li M Z, Yang L, Zhang Z D and Gao X P A 2017 *Nano Res.* **10** 1872

[101] Wiesner M, Trzaskowska A, Mroz B, Charpentier S, Wang S, Song Y, Lombardi F, Lucignano P, Benedek G, Campi D, Bernasconi M, Guinea F and Tagliacozzo A 2017 *Sci. Rep.* **7** 16449

[102] Qu D X, Che X, Kou X, Pan L, Crowhurst J, Armstrong M R, Dubois J, Wang K L and Chapline G F 2018 *Phys. Rev. B* **97** 045308

[103] Fu L 2011 *Phys. Rev. Lett.* **106** 106802

[104] Liu J W, Hsieh T H, Wei P, Duan W H, Moodera J and Fu L 2014 *Nat. Mater.* **13** 178

[105] Sundermann M, Yavaş H, Chen K, Kim D J, Fisk Z, Kasinathan D, Haverkort M W, Thalmeier P, Severing A and Tjeng L H 2018 *Phys. Rev. Lett.* **120** 016402

[106] Nam M S, Williams B H, Chen Y, Contera S, Yao S, Lu M, Chen Y F, Timco G A, Muryn C A, Winpenny R E P and Ardavan A 2018 *Nat. Commun.* **9** 56